Cell culture

Normal human osteoblasts (NHOst) were purchased from Lonza Walkersville Inc. (Walkersville, MD, USA). The standard culture of NHOst was performed using alpha minimum essential medium (Gibco, Grand Island, NY) containing 20% fetal calf serum (FCS) (Kokusai Shiyaku Co., Ltd., Tokyo Japan). The cells were maintained in incubators under standard conditions (37°C, 5 %-CO_2-95 %-air, saturated humidity). All assays were performed using alpha minimum essential medium containing 20% FCS, supplemented with 10 m*M* beta-glycerophosphate. The various SAM-covered coverslips were placed in the wells of 12-well plates and NHOsts (4×10^4 cells/well/1 mL medium) were inoculated on them. In each experiment, the medium was changed for three times and their differentiation level was evaluated after a 1-week incubation.

Proliferation and differentiation of NHOsts cultured on various SAM-covered coverslips

The proliferation of NHOst cells cultured on SAM-covered coverslips was estimated by Tetracolor One assay reagent (Seikagaku Co., Tokyo, Japan), which incorporates an oxidation–reduction indicator for detecting cellular metabolic activity. After a 1-week incubation of NHOsts, 50 μL of Tetracolor One solution was added to each test dish filled with 1 mL of a culture medium, followed by a further 2 h incubation. The absorbance of the supernatant at 450 nm was measured by μQuant spectrophotometer (Bio-tek Instruments, Inc., Winooski, VT).

Estimation of alkaline phosphatase (ALP) activity was performed according to an original procedure by Ohyama et al.[25] After estimating the proliferation of the NHOst cells cultured on the SAM-covered coverslips, the cells were washed by phosphate-buffered saline (PBS(−)), followed by the addition of 1 mL of 0.1*M* glycine buffer (pH 10.5) containing 10 m*M* $MgCl_2$, 0.1 m*M* $ZnCl_2$, and 8 m*M* *p*-nitrophenylphosphate sodium salt. After incubating the cells at room temperature for 7 min, the absorbance of the solution at 405 nm was detected using μQuant to evaluate the ALP activity of the tested cells.

The amounts of calcium deposited by the cell during a 1-week incubation were measured as follows. After fixing the cells in PBS(−) containing 3% formaldehyde, the cells were washed with PBS(−), and then 0.5 mL of 0.1*M* HCl was added to each well. The amounts of calcium dissolved in HCl were estimated using a calcium detecting kit (Calcium-C test Wako, Wako, Osaka, Japan) according to manufacturer's instruction.

Measurements of GJIC activity

NHOst cultured on SAM-covered coverslips were subjected to fluorescence recovery after photobleaching (FRAP) analysis to evaluate the effect of these surfaces on the GJIC. FRAP analysis was carried out according to the procedure of Wade et al.[26] with some modifications.[20] Briefly, NHOst were plated and incubated for 1 day on the SAM-covered coverslips. After incubated with a fluorescent dye, 5,6-carboxyfluorescein diacetate in PBS(−) containing calcium and magnesium, the cells contacting at least two other cells were subjected to FRAP analysis under Ultima-Z confocal microscope (Meridian Instruments, Okemos, MI). The cells were photobleached with a 488 nm beam, and recovery of fluorescence intensity was subsequently monitored for 4 min. The data obtained from more than seven independent cells were expressed as the average ratio of the fluorescence recovery rate to the rate obtained from NHOst cultured on a collagen-coated dish as standard experiments.

Connexin 43 mRNA expression in NHOsts

To estimate effects of the surface functional group on mRNA expression of connexin 43 protein, which plays an important role in GJIC by forming channels between neighboring cells, a real time PCR technique was applied. Briefly, total RNA from NHOsts cultured on various functional groups was isolated by RNeasy microprep kit (QIAGEN, Valencia, CA) per the manufacturer's instruction. After its reverse transcription, a real time PCR was performed utilizing the primers for connexin 43, LightCycler FastStart DNA master SYBR green I kit (Roch Applied Science, Penzberg, Germany) and LightCycler 4 (Roche Applied Science). To normalize the data, mRNA expression of a housekeeping gene, glyceraldehyde 3-phosphate dehydrogenase (GAPDH), was also determined using LightCycler primer set for GAPDH (Roche Applied Science). Primer sequences for connexin 43 are shown below:

Forward: 5′-GGGCTAATTACAGTGCAG-3′
Reverse: 5′-CATGTCCAGCAGCTAGTT-3′

Statistic analysis

All data were expressed as mean values ± standard deviation of the obtained data. The Fisher-Tukey criterion, calculated by inerSTAT-a v1.3 (freeware, published by Instituto Nacional de Enfermedades Respiratorias), was used to control for multiple comparisons and to compute the least significant difference between means.

RESULTS

Table I shows contact angle against water and elemental signal ratios of prepared coverslips covered with various SAMs. The signal ratio against a carbon signal detected in the same surface by ESCA was calculated from the signal area and the sensitivity factor of each element. If a signal area recorded on ESCA was lower than 10^3 or the calculated value was lower than 1×10^{-3}, the results were not described in the table. As shown in Table I, contact angle measurements revealed that while SAM-CH_3 had a hydrophobic surface, others SAMs except for SAM-NH_2 had hydrophilic ones compared with the intact gold-coated surface. The contact angle of SAM-OH was significantly lower than any other SAM surfaces. After a reaction from SAM-OH to SAM-OPO_3H_2, the contact angle was significantly increased, suggesting that the reaction proceeded successfully. Also as shown in Table I, the ratios of atomic concentration of nitrogen, phosphorus, and sulfur (N/C, P/C, and S/C) calculated from raw signal areas were detected only from SAM-NH_2, SAM-OPO_3H_2, and SAM-OSO_3H, respectively, indicating that

TABLE I. Surface Characterization of SAMs by Contact Angle and Elemental Signal Ratios Against Carbon

		SAMs Modifying Surfaces					
	Gold (Control)	SAM-OH	SAM-OSO_3H	SAM-COOH	SAM-OPO_3H_2	SAM- NH_2	SAM-CH_3
Contact Angle	64.4 ± 2.1	40.1 ± 14.2*,†	44.3 ± 10.2	51.7 ± 14.5	59.0 ± 13.7*	65.0 ± 9.8	102.9 ± 3.0†
Elemental signal ratios							
O/C	3.2×10^{-3}	2.9×10^{-3}	6.8×10^{-3}	4.6×10^{-3}	4.8×10^{-3}	2.2×10^{-3}	–
N/C	–	–	–	–	–	1.8×10^{-3}	–
P/C	–	–	–	–	2.1×10^{-3}	–	–
S/C	–	–	2.2×10^{-3}	–	–	–	–

* $p < 0.05$ between SAM-OH and SAM-OPO_3H_2.
† $p < 0.01$ against Au.

all desired SAM surfaces with specific functional groups were successfully prepared.

Figures 2 and 3 show light micrographs of NHOsts cultured on each SAM surface for 1 day and 1 week. When NHOsts were cultured on a gold-coated coverslip for 1 day, the number of NHOsts observed was apparently lower [Fig. 2(B)] than that on a collagen-coated culture plate [Fig. 2(A)]. After 1-week incubation, the surface of gold-coated coverslip was fully covered with NHOsts, indicating that the NHOsts could proliferate on the intact gold surface [Fig. 3(B)]. The numbers of NHOsts adhered on the gold surface with various SAMs were influenced by the functional groups covering the SAMs as follows. Less NHOsts could adhere on a SAM-CH_3, the most hydrophobic surface among the SAM surfaces used in this study, than those on the gold surface [Figs. 2(C) and 3(C)]. The NHOsts on the SAM-CH_3 were tended to aggregate after 1-day culture [Fig. 2(C)] and likely to detach from the surface during 1-week culture as no aggregates and few stretched NHOsts were observed after 1 week [Fig. 3(C)]. On the other hand, NHOsts adhered on other SAM surfaces such as SAM-COOH, SAM-OH, SAM-OPO_3H_2 and SAM-OSO_3H could be observed more than on the gold surface, as shown in Figure 1(D,E,G,H). Judging from the number of nodules observed in Figure 3, it is likely that there is no effect of functional groups in between the hydrophilic SAM surfaces on differentiation level of NHOsts.

Table II summarizes the relative amount of cell number, ALP activity, and the deposited calcium of NHOsts after 1-week culture on various SAMs. Although differentiation levels of NHOsts on hydrophilic functional groups of SAM were not significantly different by the observation of the nodule number (Fig. 3), the functional groups apparently influenced both ALP activity of the NHOsts and the amount of deposited calcium as well as the cell number ratio adhering on the surface as shown in Table II. When NHOsts were cultured on SAM-CH_3 surface, not only the cell number but also their ALP activity were low and the amount of deposited calcium per cell were under detection limit. On the contrary, when NHOsts were cultured on SAM-OH, SAM-COOH, or SAM-NH_2, the cell number, the ALP activity and the deposited calcium amounts per cell were not significantly different from those observed on a gold surface. Interestingly, when NHOsts were cultured on SAM-OPO_3H_2 or SAM-OSO_3H, their ALP activity and the amounts of calcium deposition per cell increased although the cell number ratio was about one-third to half of that observed on a gold surface.

To estimate the effects of functional groups on another cell function, GJIC level of NHOsts on various SAM surfaces were measured after 1-day incubation (Table III). In addition, expression levels of connexin 43 mRNA in NHOsts on the various functional groups were measured by real-time PCR (Fig. 4). Although it was observed that their differentiation level was influenced by the functional group on SAM surfaces, statistical differences in neither the GJIC level nor the expression level of connexin 43 mRNA during 1-week culture were observed among the SAM surfaces tested in comparison with that of NHOsts on a collagen-coated dish at the same time period of their culture.

DISCUSSION

Several studies have been reported that surface chemical properties are responsible for behavior of attached cells, for example, their adhesion, proliferation, and differentiation on the surface as well as surface topography such as microfabricated grooves and pits.[9–12,27,28] Usually, a cell adheres not directly on a surface of a material but on preadsorbed proteins on the material, originally contained in the culture medium. Interaction of the preadsorbed proteins with a material surface is important in cell attachment and protein adsorption is influenced by surface properties, such as chemical composition, surface charge, and a hydrophilicity/hydrophobicity balance of surface.[9] Therefore, SAM is an ideal surface to investigate effects of the chemical and physico–chemical property on cell behavior as the surface covered by single chemical group can be prepared easily.

Changes in contact angles and elemental signal ratio against carbon signals of the prepared SAM surfaces (Table I) indicated that SAM surfaces covered with various chemical groups could be prepared successfully by the methods described in "Materials and Methods" section. Although chlorosulfonic acid is a common reagent to convert hydroxyl groups of SAM-OH to sulfate group,[29] we used DMF-SO_3 for the preparation of SAM-OSO_3H in this study. In the trial of substitution reaction by chlorosulfonic acid, it was found to be difficult to remove all by-products adsorbed on the coverslip without detaching a gold coating, thus modest

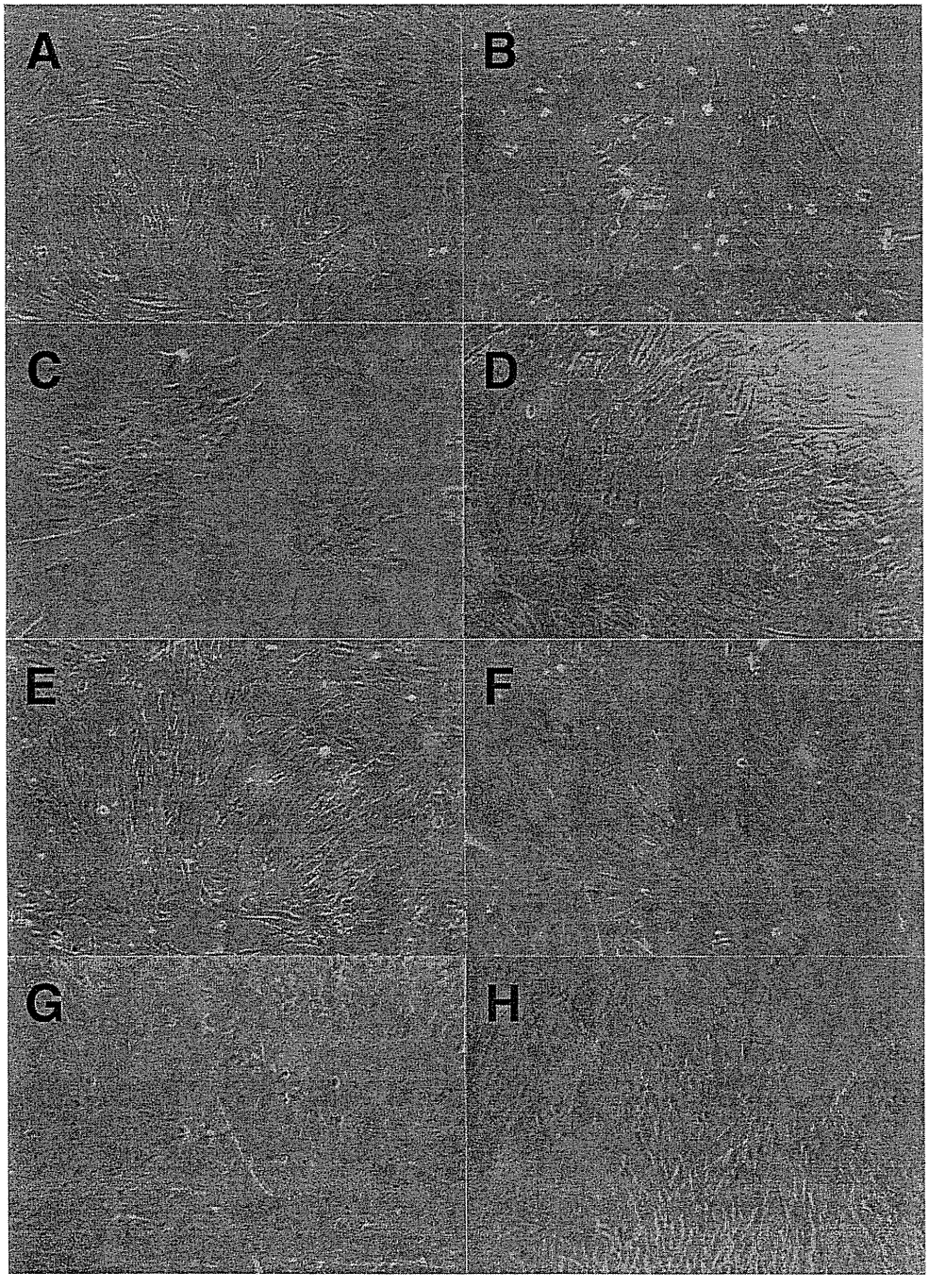

FIGURE 2. Light micrograph of NHOsts cultured on various SAM surfaces for 1 day. (Original magnification is ×40.) NHOsts were cultured on a collagen-coated dish (A), gold-coated coverslip (B), SAM-CH_3 (C), SAM-COOH (D), SAM-OH (E), SAM-NH_2 (F), SAM-OPO_3H_2 (G), and SAM-OSO_3H (H). [Color figure can be viewed in the online issue, which is available at www.interscience.wiley.com.]

condition reaction, which is often applied for sulfation reaction of hydroxyl groups in polysaccharides with fewer by-products, was employed. In fact, an apparent S/C signal was detected as shown in Table I, indicating the sulfate group was successfully introduced to the surfaces by the employed reaction in good yield.

Effect of chemical groups on cell attachment has been studied as well as protein adsorption utilizing SAM. It has been reported that the number of cell adhering on various surfaces is influenced by the physico-chemical properties of the surfaces such as hydrophilic/hydrophobic balance, which is closely related to contact angles.[11,12,27,30–33] In this study, modification of the gold surface with SAM changed the number of NHOsts adhering on the surface depending on the functional groups of the SAM (Fig. 2). Less NHOsts could adhere on a SAM-CH_3, the most hydrophobic surface among the prepared SAM surfaces, than those on the gold surface. The NHOsts observed on it were tend to aggregate

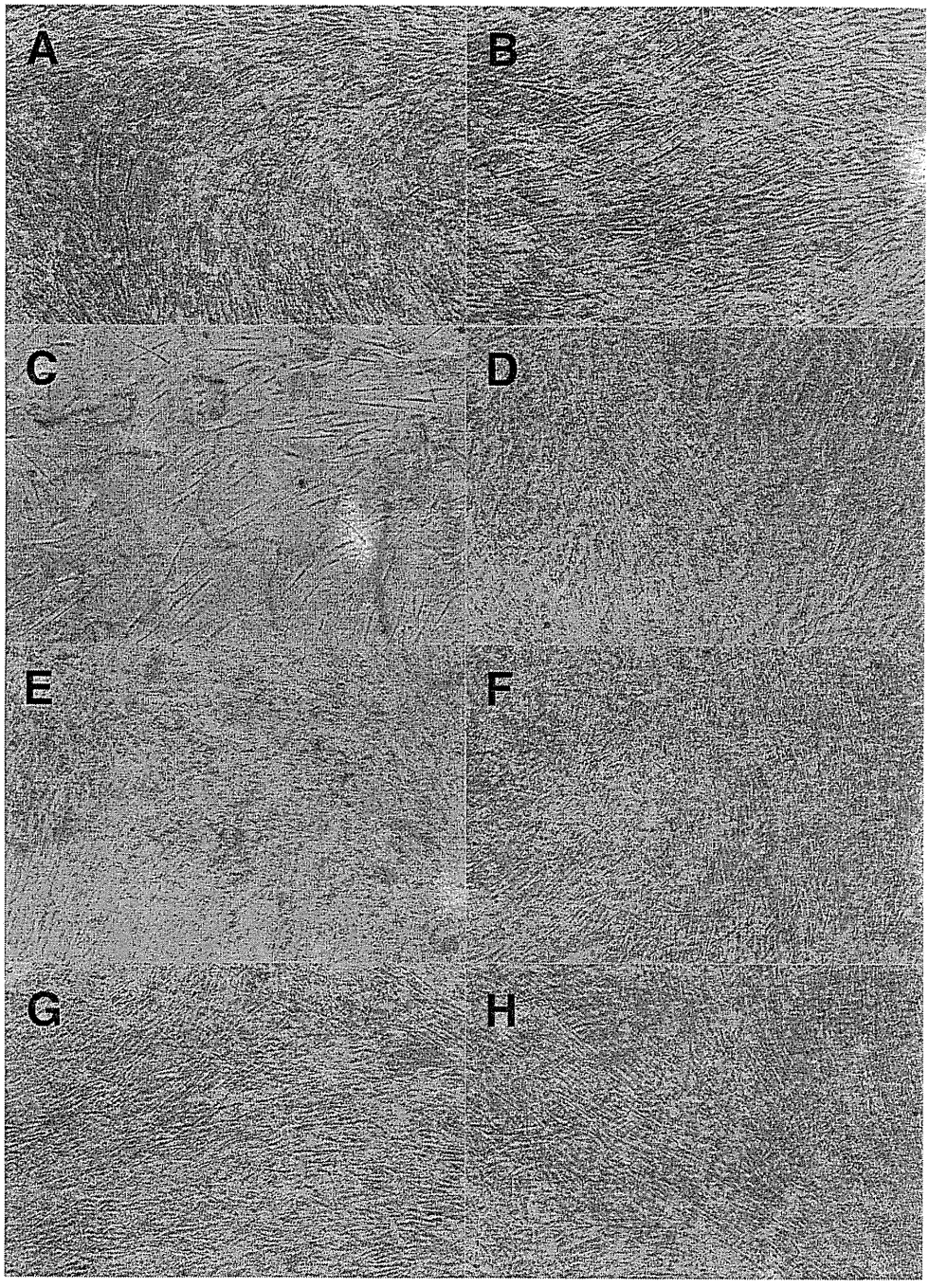

FIGURE 3. Light micrograph of NHOsts cultured on various SAM surfaces for 7 days. (Original magnification is ×40.) NHOsts were cultured on a collagen-coated dish (A), gold-coated coverslip (B), SAM-CH_3 (C), SAM-COOH (D), SAM-OH (E), SAM-NH_2 (F), SAM-OPO_3H_2 (G), and SAM-OSO_3H (H). [Color figure can be viewed in the online issue, which is available at www.interscience.wiley.com.]

and likely to detach from it during 1-week culture as no aggregates and a few stretched NHOsts were observed on it as shown in Figure 3. On the other hand, NHOsts could adhere on other SAM surfaces more than on the gold surface, indicating that the surfaces covered with functional groups such as amino, carboxyl, hydroxyl, phosphate, and sulfate groups have a suitable hydrophilic/hydrophobic balance not to interfere cell adhesion them. As adhesion and spreading behaviors of osteoblasts on materials have been reported to depend on vitronectin and fibronectin primarily adsorbed on the surfaces,[34,35] it may be indispensable to investigate an interaction between various functional groups and these two proteins influencing there adsorption behavior and possible conformation changes to clarify the mechanism of cell adhesion on the interacted-functional groups more precisely.

The ALP activity and deposited calcium amount were measured for estimating differentiation level of NHOsts

TABLE II. The Cell Number, Alkaline Phosphatase Activities, and Deposited Calcium Amounts of NHOsts Cultured on Several Kinds of Prepared SAM Surfaces after 1-week Incubation

Samples	The Cell Number Ratio (%)	$\frac{\text{ALP Activity}}{\text{The Cell Number}}$ (%)	$\frac{\text{Calcium Amounts}}{\text{The Cell Number}}$ (μg/ratio)
Gold	100.0 ± 4.9	100.0 ± 10.0	8.1 ± 1.6
SAM-OH	107.8 ± 2.2	119.7 ± 6.4	8.7 ± 2.3
SAM-OSO_3H	50.8 ± 15.4*	150.1 ± 55.0	33.4 ± 13.5
SAM-COOH	93.2 ± 33.9	100.2 ± 6.8	11.6 ± 2.5
SAM-OPO_3H_2	37.5 ± 4.2*	147.5 ± 9.4	57.0 ± 25.2**
SAM-NH_2	106.1 ± 8.6	112.1 ± 4.3	8.5 ± 1.1
SAM-CH_3	17.1 ± 10.3*	34.8 ± 26.0*	Not detected
Collagen-dish	156.7 ± 3.1†	119.3 ± 6.0	15.5 ± 2.9

The cell number and the alkaline phosphatase activities were expressed as a ratio of against those on gold-coated coverslip. Both the alkaline phosphatase activities and the calcium amounts were normalized by the cell number.

* $p < 0.05$ against "Gold" and SAM-COOH group, and $p < 0.01$ against other SAM.

** $p < 0.05$ against "Gold."

† $p < 0.01$ against all other groups.

cultured on prepared SAM surfaces (Table II). When NHOsts were cultured on SAM-CH_3 surface, not only the cell number but also their ALP activity decreased and the amounts of deposited calcium per cell were not detected. This suggests that NHOsts cannot maintain their differentiation level when they cannot adhere on the surface. When NHOsts were cultured on SAM-OH, SAM-COOH, or SAM-NH_2, their number, ALP activity and deposited calcium amounts per cell were almost the same as those observed on a gold surface. These indicate that a surface property that affects cell adhesion level is a one of factors to regulate differentiation level of NHOst. Interestingly, when NHOsts were cultured on SAM-OPO_3H_2 or SAM-OSO_3H, ALP activity of NHOsts and the amounts of calcium deposition per cell increased although the cell number ratio was about a one-third to a half of that observed on a gold surface. Tanahashi and Matsuda have reported that a surface covered with negatively charged chemical groups enhances the growth rate of apatite when it was soaked in a simulated body fluid because of interaction between calcium ion and the surface.[23] Interestingly, an apatite growth rate on SAM-OPO_3H_2 has been reported to be higher than that on SAM-COOH,[23] suggesting an equilibrium constant of the functional groups, which determines their negative charge level in physiological pH, affects strength of the interaction. In this study, SAM-COOH cultured with NHOsts showed almost the same calcium deposition as SAM-OH and gold surface, while SAM-OPO_3H_2 and SAM-OSO_3H showed calcium deposition 4 to 7 times as much as other surfaces tested. In addition, ALP activity of NHOsts on these two SAM surfaces was higher than any other surfaces including collagen-coated dish, which is normally utilized for a culture of NHOsts. Table I indicates that contact angle of SAM-OH is almost similar to that of SAM-OSO_3H and there are no statistical differences among contact angles of 3 SAMs, SAM-OSO_3H, SAM-COOH, and SAM-OPO_3H_2. Therefore, these findings suggest that chemical composition of the surfaces, which determines its ionic charge and zeta potentials of surfaces in physiological pH, may be one of key factors to regulate differentiation level of osteoblasts more than their hydrophilic/hydrophobic balance. As different ionic charge of SAM surfaces has been reported to influence protein adsorption as well as their hydrophilic/hydrophobic balances,[36] it is necessary to evaluate actual zeta potentials of prepared SAM surfaces in physiological pH before investigating the interaction between various functional groups and proteins including vitronectin and fibronectin, which may provide valuable information of effects of the functional groups on the cell differentiation level as well.

Although the differentiation level of NHOsts was influenced by the functional groups on SAM surfaces, their GJIC level after 1-day culture were almost the same as that of NHOsts cultured on a collagen-coated dish as a control experiment, irrespective of the type of functional group (Table III). This indicates that NHOsts interacting with these functional groups can maintain their homeostasis, irrespective of the kind of the functional group. Although GJIC has been reported to play a role in differentiation of osteoblasts,[37,38] the effect of the functional group on differentiation level of NHOsts observed in this study may be

TABLE III. Gap Junctional Intercellular Communication Activity of NHOst on Various SAM Surfaces after 1-day Incubation Measured by FRAP Analysis Technique

	Collagen-Coated Dish (control)	Gold	SAMs Modifying Surfaces					
			SAM-OH	SAM-OSO_3H	SAM-COOH	SAM-OPO_3H_2	SAM-NH_2	SAM-CH_3
GJIC activity (Ratio vs. control)	1.00 ± 0.38	1.00 ± 0.69	1.11 ± 0.46	0.92 ± 0.47	0.87 ± 0.41	1.12 ± 0.41	1.15 ± 0.46	1.24 ± 0.54

All values were calculated as a ratio of the activity against that obtained from NHOsts on a collagen-coated culture dish (control). (n = 12–14).

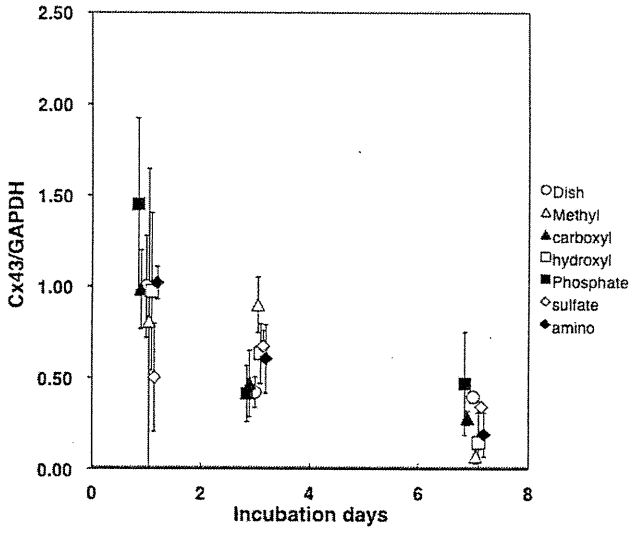

FIGURE 4. Expression levels of connexin 43 mRNA in NHOsts cultured on various SAM surfaces ($n = 3$). The expression levels of the connexin 43 mRNA were normalized by GAPDH mRNA expression level estimated from the same samples of total RNA and expressed as a ratio against the expression level in NHOsts on a collagen-coated culture dish after 1-day culture. NHOsts were cultured on a collagen-coated dish (open circle), SAM-CH_3 (open triangle), SAM-COOH (closed triangle), SAM-OH (open square), SAM-OPO_3H_2 (closed square), SAM-OSO_3H (open diamond), and SAM-NH_2 (closed diamond).

independent of their GJIC function. It was also expected that GJIC of NHOsts on SAM-CH_3 would be different from others since less NHOst proliferation on the SAM suggested a possible perturbation in homeostasis of the NHOsts. Decrease in the cell number on the SAM after 1-week incubation, however, made GJIC measurement unable because few cells contacting with two other neighboring cells were found. On the other hand, the GJIC after 1-week culture did not show any statistical differences between NHOsts on other tested SAM surfaces and those on a collagen-coated culture dish (data not shown). In addition, Figure 4 has revealed that surface functional groups of SAM do not affect mRNA expression level of connexin 43 during 1-week culture, indicating that the functional group do not affect signal cascades of connexin 43 expression in NHOsts. To study effects of the functional group as well as hydrophilic/hydrophobic balance of the surface on GJIC more in detail, changes in GJIC level of cells on the surfaces are under investigation utilizing metabolic cooperation assay system. Results of the study will be reported in near future. However, this study suggests that an enhancement of differentiation level of NHOsts induced by phosphorylated or sulfate group on the surface is triggered by a direct interaction between the chemical group and NHOsts, followed by signal cascades in which GJIC does not participate. In fact, sulfated polysaccharides have been reported to affect expression of several genes relating to cell differentiation,[15] but a mechanism of the sulfated group to affect the expression of these genes remains to be clarified. The details of the interaction and the signal cascades will be clarified in future studies.

CONCLUSIONS

This study suggests that the functional groups covering surface have the potential to control attachment, proliferation, and differentiation of NHOsts cultured on it. Figures of NHOsts after 1-day culture and the cell numbers estimated after 1-week culture indicate that hydrophilic/Hydrophobic balance of the surfaces may be one of key factors to regulate attachment and proliferation of NHOsts on the surfaces. Although the proliferation level decreased, the surface covered with either phosphate or sulfate group showed an enhancement in differentiation level of cultured NHOsts through unidentified signal cascades triggered by these functional groups and independent of GJIC. This suggests that ionic charge level of the functional groups is one of key factors to regulate osteogenic differentiation on the surfaces more than hydrophilic/hydrophobic balance of the surfaces. Further studies are necessary for clarifying the mechanisms of different differentiation levels of NHOsts induced by interaction with the functional groups as well as for future applications of SAMs in the fields of medical devices and tissue engineering.

ACKNOWLEDGMENTS

Authors are grateful to Professor Toshiaki Enoki and Associate Professor Ken-ichi Fukui (currently Professor of Osaka University), Tokyo Institute Technology for their kind permission to utilize electron-beam evaporation equipment for chromium precoating. Authors are also grateful to Dr. Rumi Sawada, Division of Medical Devices, NIHS, Japan, for her kind support in real-time PCR experiments.

REFERENCES

1. Adams JC, Watt FM. Regulation of development and differentiation by the extracellular matrix. Development 1993;117:1183–1198.
2. Peterson WJ, Tachiki KH, Yamaguchi DT. Extracellular matrix alters the relationship between thymidine incorporation and proliferation of MC3T3-E1 cells during osteogenesis *in vitro*. Cell Prolif 2002;35:9–22.
3. Hirano Y, Okuno M, Hayashi T, Goto K Nakajima A. Cell-attachment activities of surface immobilized oligopeptides RGD, RGDS, RGDV, RGDT, and YIGSR toward five cell lines. J Biomater Sci Polym Ed 1993;4:235–243.
4. Alsberg E, Anderson KW, Albeiruti A, Rowley JA, Mooney DJ. Engineering growing tissues. Proc Natl Acad Sci 2002;99: 12025–12030.
5. Bisson I, Kosinski M, Ruault S, Gupta B, Hilborn J, Wurm F, Frey P. Acrylic acid grafting and collagen immobilization on poly(ethylene terephthalate) surfaces for adherence and growth of human bladder smooth muscle cells. Biomaterials 2002;23:3149–3158.
6. Nakaoka R, Tsuchiya T. Neural differentiation of midbrain cells on various protein-immobilized polyethylene films. J Biomed Mater Res A 2003;64:439–446.
7. Masters KS, Shah DN, Walker G, Leinwand LA, Anseth KS. Designing scaffolds for valvular interstitial cells: Cell adhesion and function on naturally derived materials. J Biomed Mater Res A 2004;71:172–180.
8. Kong HJ, Boontheekul T, Mooney DJ. Quantifying the relation between adhesion ligand-receptor bond formation and cell phenotype. Proc Natl Acad Sci 2006;103:18534–18539.
9. Wilson CJ, Clegg RE, Leavesley DI, Pearcy MJ. Mediation of biomaterials-cell interactions by adsorbed proteins: A review. Tissue Eng 2005;11:1–18.
10. Ulman A. Formation and structure of self-assembled monolayers. Chem Rev 1996;96:1533–1554.

11. Mrksich M, Whitesides GM. Using self-assembled monolayers to understand the interactions of man-made surfaces with proteins and cells. Annu Rev Biophys Biomol Struct 1996;25:55–78.
12. Senaratne W, Andruzzi L, Ober CK. Self-assembled monolayers and polymer brushes in biotechnology: Current applications and future perspectives. Biomacromol 2005;6:2427–2448.
13. Fujimoto H, Yoshizako S, Kato K, Iwata H. Fabrication of cell-based arrays using micropatterned alkanethiol monolayers for the parallel silencing of specific genes by small interfering RNA. Bioconjugate Chem 2006;17:1404–1410.
14. Shin SK, Yoon HJ, Jung YJ, Park JW. Nanoscale controlled self-assembled monolayers and quantum dots. Curr Opin Chem Biol 2006;10:423–429.
15. Nagira T, Nagahata-Ishiguro M, Tsuchiya T. Effect of sulfated hyaluronan on keratinocyte differentiation and Wnt and Notch gene expression. Biomaterials 2007;28:844–850.
16. Maio AD, Vaga VL, Contreras JE. Gap junctions, homeostasis, and injury. J Cell Physiol 2002;191:269–282.
17. Tsuchiya T, Hata H, Nakamura A. Studies on the tumor-promoting activity of biomaterials: Inhibition of metabolic cooperation by polyetherurethane and silicone. J Biomed Mater Res 1995;29: 113–119.
18. Tsuchiya T, Takahara A, Cooper SL, Nakamura A. Studies on the tumor-promoting activity of polyurethanes: Depletion of inhibitory action of metabolic cooperation on the surface of a polyalkyleneurethane but not a polyetherurethane. J Biomed Mater Res 1995;29:835–841.
19. Nakaoka R. Tsuchiya T, Sakaguchi K, Nakamura A. Studies on *in vitro* evaluation for the biocompatibility of various biomaterials: Inhibitory activity of various kinds of polymer microspheres on metabolic cooperation. J Biomed Mater Res 2001;57:279–284.
20. Nakaoka R, Tsuchiya T, Nakamura A. The inhibitory mechanism of gap junctional intercellular communication induced by polyethylene and the restorative effects by surface modification with various proteins. J Biomed Mater Res 2001;57:567–574.
21. Nagahata M, Nakaoka R, Teramoto A, Abe K, Tsuchiya T. The responses of normal human osteoblasts to anionic polysaccharide polyelectrolyte complexes. Biomaterials 2005;26:5138–5144.
22. Nakaoka R, Tsuchiya T. Enhancement of differentiation and homeostasis of human osteoblasts by interaction with hydroxyapatite in microsphere form. Key Eng Mater 2006;309–311:1293–1298.
23. Tanahashi M, Matsuda T. Surface functional group dependence on apatite formation on self-assembled monolayers in a simulated body fluid. J Biomed Mater Res 1997;34:305–315.
24. Hamano T, Chiba D, Nakatsuka K, Nagahata M, Teramoto A, Kondo Y, Hachimori A, Abe K. Evaluation of a polyelectrolyte complex (PEC) composed of chitin derivatives and chitosan, which promotes the rat calvarial osteoblast differentiation. Polym Adv Technol 2002;13:46–53.
25. Ohyama M, Suzuki N, Yamaguchi Y, Maeno M, Otsuka K, Ito K. Effect of enamel matrix derivative on the differentiation of C2C12 cells. J Periodontol 2002;73:543–550.
26. Wade MH, Trosko JE, Schlindler M. A fluorescence photobleaching assay of gap junctional-mediated communication between human cells. Science 1986;232:525–528.
27. Ito Y. Surface micropatterning to regulate cell functions. Biomaterials 1999;20:2333–2342.
28. Hamilton DW, Brunette DM. The effect of substratum topography on osteoblast adhesion mediated signal transduction and phosphorylation. Biomaterials 2007;28:1806–1819.
29. Bertilsson L, Liedberg B. Infrared study of thiol monolayer assemblies on gold: Preparation, characterization, and functionalization of mixed monolayers. Langmuir 1993;9:141–149.
30. Mrksich M, Chen CS, Xia Y, Dike LE, Ingber DE, Whitesides GM. Controlling cell attachment on contoured surfaces with self-assembled monolayers of alkanethiolates on gold. Proc Natl Acad Sci 1996;93:10775–10778.
31. McClary KB, Ugarova T, Grainger DW. Modulating fibroblast adhesion, spreading, and proliferation using self-assembled monolayer films of alkylthiolates on gold. J Biomed Mater Res 2000;50: 428–439.
32. Scotchford CA, Gilmore CP, Cooper E, Leggett GJ, Downes S. Protein adsorption and human osteoblasts-like cell attachment and growth on alkylthiol on gold self-assembled monolayers. J Biomed Mater Res A 2002;59:84–99.
33. Cox JD, Curry MS, Skirboll SK, Gourley PL, Sasaki DY. Surface passivation of a microfluidic device to glial cell adhesion: A comparison of hydrophobic and hydrophilic SAM coatings. Biomaterials 2002;22:929–935.
34. Howlett CR, Evans MDM, Walsh WR, Johnson G, Steele JG. Mechanism of initial attachment of cells derived from human bone to commonly used prosthetic materials during cell culture. Biomaterials 1994;15:213–222.
35. Kilpadi KL, Chang PL, Bellis SL. Hydroxyapatite binds more serum proteins, purified integrins, and osteoblast precursor cells than titanium or steel. J Biomed Mater Res A 2001;57:258–267.
36. Kidoaki S, Matsuda T. Mechanistic aspects of protein/material interactions probed by atomic force microscopy. Colloids Surf B 2002;23:153–163.
37. Lecanda F, Towler DA, Ziambaras K, Cheng SL, Koval M, Steinberg TH, Civitelli R. Gap junctional communication modulates gene expression in osteoblastic cells. Mol Biol Cell 1998;9: 2249–2258.
38. Donahue HJ, Li Z, Zhou Z, Yellowley CE. Differentiation of human fetal osteoblastic cells and gap junctional intercellular communication. Am J Physiol Cell Physiol 2000;278:C315–C322.

///VSP///

Journal of Biomaterials Science 21 (2010) 1957–1970

Journal of BIOMATERIALS SCIENCE
brill.nl/jbs

Self-Organization of the Compositional Gradient Structure in Hyaluronic Acid and Poly(N-isopropylacrylamide) Blend Film

Bayar Hexig [a,*], Kazuo Isama [b], Yuji Haishima [b], Yoshio Inoue [a], Toshie Tsuchiya [b,c] and Toshihiro Akaike [a,d]

[a] Department of Biomolecular Engineering Graduate School of Bioscience and Biotechnology, Tokyo Institute of Technology, 4259 Nagatsuta-cho, Midori-ku, Yokohama-shi 222-8501, Japan
[b] Division of Medical Devices, National Institute of Health Sciences, Kamiyoga, 1-18-1 Setagaya-ku, Tokyo 158-8501, Japan
[c] Medical center for Translational Research, Osaka University Hospital, 2-15 Yamadaoka, Suita, Osaka 565-0871, Japan
[d] Frontier Research Center, Tokyo Institute of Technology, 4259 Nagatsuta-cho, Midori-ku, Yokohama-shi 222-8501, Japan

Received 13 May 2010; accepted 23 August 2010

Abstract

A compositional gradient structure in hyaluronic acid (HA) and poly(N-isopropylacrylamide) (PIPAAm) blend film was self-organized from a homogeneous aqueous solution in a plasma-treated polystyrene dish (PTPSD), and the formation mechanisms of the gradient structure were studied by casting the same solution on PTPSD and a non-treated polystyrene dish (NTPSD) under ambient and vacuum conditions. The formation of a compositional gradient structure in HA/PIPAAm blend film was confirmed by scanning electron microscopy, energy dispersive X-ray (EDX) mapping analysis and step-scan photoacoustic Fourier transformed infrared spectroscopy (PAS–FT-IR) measurements. The EDX mapping measurements for Na element revealed that the HA component gradually decreases from the dish-side to the air-side of the film cast on PTPSD, while for the film cast on NTPSD no such obvious change was observed on the cross-section. Further studies on the films prepared on PTPSD and NPTPSD under ambient and vacuum conditions demonstrated that the hydrophilic interaction and the solvent evaporation rate were the most significant factors leading to the formation of a compositional gradient structure in the HA/PIPAAm blend system.

Keywords

Self-organization, FGM, hyaluronic acid, poly(N-isopropylacrylamide)

* To whom correspondence should be addressed. E-mail: bhexig@bio.titech.ac.jp

DOI:10.1163/092050610X528589

1. Introduction

Biomimetic and bioinspired optimal structures combining bioresorbable, bioactive and other advanced properties are expected for the next generation of biomaterials [1–3]. Inspired by nature, to reveal the relationship between structure and functionality of biological materials has been emphasized in the biomaterials research field, and self-organization of a polymeric system has been recognized as a key challenge for producing functional materials that combine several properties and the inherent beauty of ordered structures [4, 5]. In nature, gradient biological structures exist most commonly, such as the structure of bamboo [6], shells, teeth, bones, tendon and extracellular matrix (ECM) [7]. Man-made functionally gradient materials (FGMs) have been developed for combining irreconcilable properties within a single material and have been widely incorporated in metal/ceramic and organic/inorganic material fields for increasing the structural complexity and combining different functionality [8–10].

Recently, there have been many efforts to develop polymeric FGMs with unique properties and advanced functions that are inaccessible in conventional uniform systems [11, 12]. Many preparation approaches have been developed to generate a polymeric functionally gradient structure during homogenization or segregation processes [13–16]. Despite these efforts made recently to generate polymeric FGMs, characterization of their gradient structure, physico-chemical properties and elucidation of formation mechanisms still remain to be explored. Previously, the spontaneous formation of a chitosan/poly(vinyl alcohol) compositional gradient structure on a aluminum dish from a homogeneous aqueous solution was reported, and the gradient film was found to show some unique physical properties compared to a homogeneous blend film which was prepared on a Teflon dish [12]. However, there is still no detailed understanding of the formation mechanisms of such a compositional gradient structure spontaneously formed on a aluminum dish. It requires both the hydrophilic and hydrophobic properties incorporated into the same material surfaces, but it is extremely difficult to control these on the metallic substrate's surface because oxidation occurs at any given moment in ambient conditions.

Plasma technology can add functional groups to a surface of organic and inorganic materials at the molecular level, changing surface chemistries to obtain increased bond strength, hydrophilicity, permeability, and activating and changing surfaces from hydrophobic to hydrophilic without affecting the bulk properties. In the present study, we show a compositional gradient structure in a HA/PIPAAm blend film self-organized during the solvent evaporation process on a oxygen-plasma treated polystyrene dish (PTPSD), while on the non-treated polystyrene dish (NTPSD) a nearly homogenous blend film was formed at ambient condition.

HA is a naturally occurring linear polysaccharide, widely distributed in the body as a component of ECM of connective tissues, and recently HA-based biomaterials have been utilized for a variety of clinical applications and tissue engineering of skin, cartilage tissue and bone, based upon its specific properties, excellent biocompatibility and bioactivity [17–21]. PIPAAm is a synthetic polymer which has a sharp

and reversible phase transition at approx. 32°C and is applicable in tissue engineering as a functional hydrogel and as a cell sheet [22, 23]. It is interesting to develop a novel biomaterial combining the biocompatibility, bioactivity of HA and the inherent thermal responsibility of PIPAAm in the tissue engineering field. For improving the biocompatibility of PIPAAm hydrogel, intensive studies have been done to develop a series of thermosensitive co-polymers by coupling carboxylic end-capped PIPAAm to HA through amide bond linkages [24–26]. In the present study, we aimed to prepare a composite material of HA and PIPAAm with a gradual change in chemical composition which combines not only the inherent properties of two components, but also those of their complex with various compositions. It is expected that such a compositional gradient material could provide rather advanced and new properties compared to the conventional composite material with a given compositional ratio of the components. A compositional gradient structure in bioactive sodium hyaluronic acid (HA) and thermal-responsive poly(N-isopropylacrylamide) (PIPAAm) blend film was simply self-organized from a homogeneous aqueous solution on a plasma-treated polystyrene dish (PTPSD) at room temperature. The formation mechanism was studied by casting the same solution on PTPSD and non-treated polystyrene dish (NTPSD) under ambient and vacuum conditions at room temperature. Our findings demonstrate that the hydrophilic interaction with substrate and the solvent evaporation rate were the most significant factors for the formation of the compositional gradient structure in the HA/PIPAAm blend system.

2. Materials and Methods

2.1. Materials

2.1.1. Film Preparation

A 1 wt% HA solution was prepared by dissolving powder HA (weight-average molecular weight 1 680 000 by GPC, Life Core Biomedical) in distilled water with stirring for 24 h. A 1 wt% PIPAAM solution was prepared by diluting 15 wt% PIPAAm (weight-average molecular weight 220 000 by GPC, Kohjin) aqueous solution with distilled water with stirring for 24 h. Thereafter the 1 wt% HA and 1 wt% PIPAAm solutions were mixed together at the same weight ratio and stirred further for 24 h before casting on PTPSD and NTPSD in ambient and vacuum conditions. For the preparation of films from the same amount of solution with the same concentration, it needed 48 h in ambient conditions, while it needed only 12 h in vacuum. All resulting films were heated at 80°C under vacuum condition for 5 h before evaporation of the remained water in the film and characterization.

2.2. Plasma Treatment of the Polystyrene Dish

The plasma treatment was performed with a SWP-101EX (Nissin), using low-pressure region output power of the microwave oscillator at 2.0 kW; the polystyrene dishes were set on the sample stage which is 15 cm below the reactor. The oxygen

discharge was utilized and the oxygen was filled at a rate of 500 cc/min at a pressure of 70 Pa. Plasma irradiation was performed for 15 s.

2.3. X-Ray Photoelectron Spectroscopy (XPS)

The XPS analyses were performed with an ESCA-3200 spectrometer (Shimadzu), using a magnesium Kα X-ray source (1253.6 eV). The high-resolution spectra of the C_{1s}, O_{1s} and Na_{1s} regions were recorded with a pass energy of 75 eV at 45° take-off angle.

2.4. Scanning Electron Microscopy (SEM) and Energy Dispersive X-Ray (EDX) Analysis

A JSM-5800LV (JEOL) equipped with an EX-23000BU EDX detector was used to analyze the freeze-fractured cross-section geometry, the chemical composition and element mapping measurements. The samples were fractured at liquid-nitrogen temperature, and sputtered with gold before taking micrographs.

2.5. Step-Scan Photoacoustic Fourier Transformed Infrared Spectroscopy (PAS–FT-IR)

PAS–FT-IR spectra measurements were carried out on a JIR-SPX200 FT-IR spectrometer (JEOL) equipped with a MTEC 300 photoacoustic cell (MTEC Photoacoustic). Prior to the start of the penetration experiment the cell was purged with helium for 30 s.

3. Results and Discussion

3.1. Surface Analysis of the Compositional Gradient Film

Figure 1 shows the molecular structures and XPS spectra of pure PIPAAm, pure HA, and the difference of chemical compositions between two surfaces of the blend film cast from homogeneous aqueous solution with the same compositional fraction of HA/PIPAAm (50%/50%) on PTPSD at room temperature, and the C_{1s} and Na_{1s} core level regions are also shown. For pure PIPAAm, the C_{1s} spectrum is decomposed by peak fitting to two components at 285.0 and 287.9 eV, corresponding to the hydrocarbon (H*C*) (including carbon singly bound to nitrogen (*C*N)) and the carbon atom in carbonyl group environments, respectively. The high-resolution C_{1s} spectrum of HA is decomposed to four peaks at 285.0 ± 0.1, 286.6 ± 0.1, 288.1 ± 0.1 and 289.5 ± 0.1 eV, corresponding to the H*C* (including *C*N), carbon singly bound to oxygen (*C*O), carbon doubly bonded to oxygen (O*C*O) (including amide and carboxylate ion carbon atoms (*C*ON and *C*OO)), and finally carbon in an ester environment (COOR), respectively, resulting in a very close match to the experimentally observed spectrum. Both the high-resolution XPS spectra in C_{1s} and Na_{1s} core level regions were obviously different between two surfaces of the HA/PIPAAm film cast on PTPSD at room temperature. The spectra of the air-side surface are close to that of pure PIPAAm (Fig. 1c) and the spectra of the dish-side surface are close to that

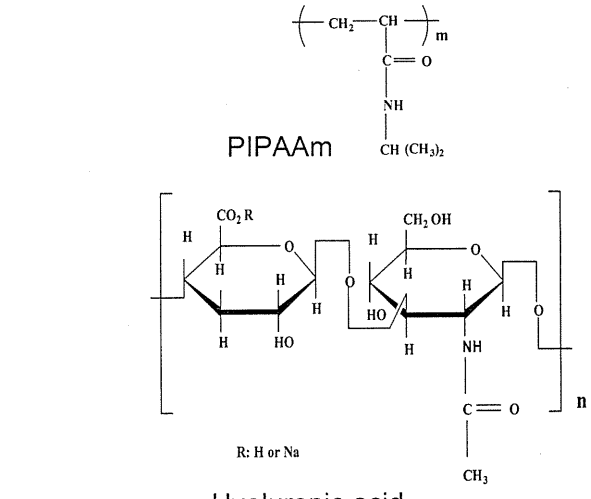

(a)

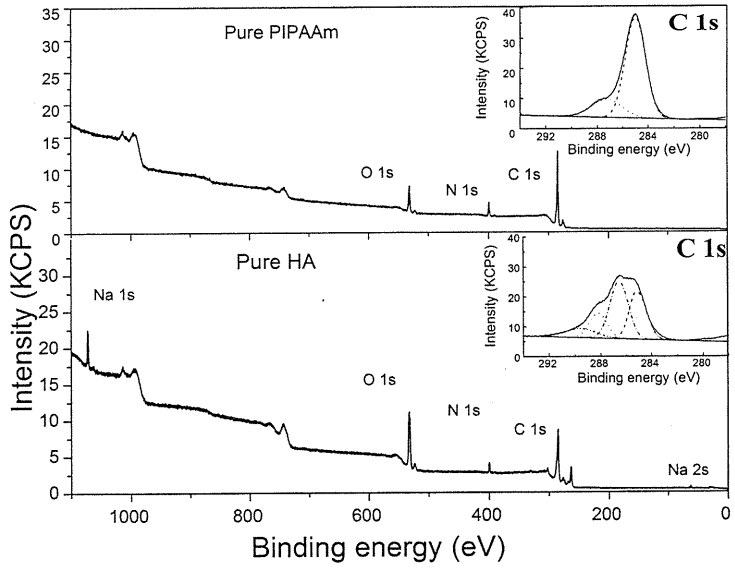

(b)

Figure 1. (a) Molecular structure of pure PIPAAm and pure HA. (b) XPS spectra of pure PINPAAm and pure HA. The inset shows the corresponding magnification of the C_{1s} core level regions and the results resolved by the curve-fitting program. Dashed line, HC; dash-dotted line, CO; dotted line, OCO; dash-dot-dotted line, CON or COO; short dashed line, baseline; short dash-dotted line, curve-fitted results; solid line, experimental results. (c, d) XPS spectra of the air-side and dish-side surfaces of the film cast on PTPSD in ambient conditions, respectively. The insets are the corresponding Na_{1s} core level regions.

of pure HA (Fig. 1d). It implies that the cross-section of the film may form a gradient structure in the HA/PIPAAm blend composition along the thickness direction.

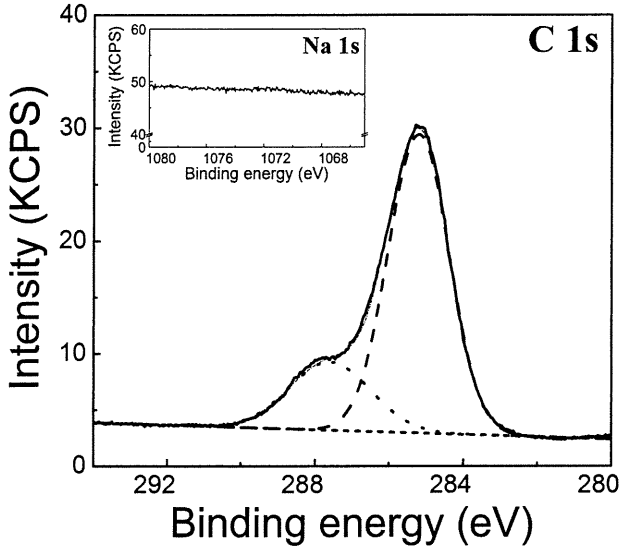

(c)

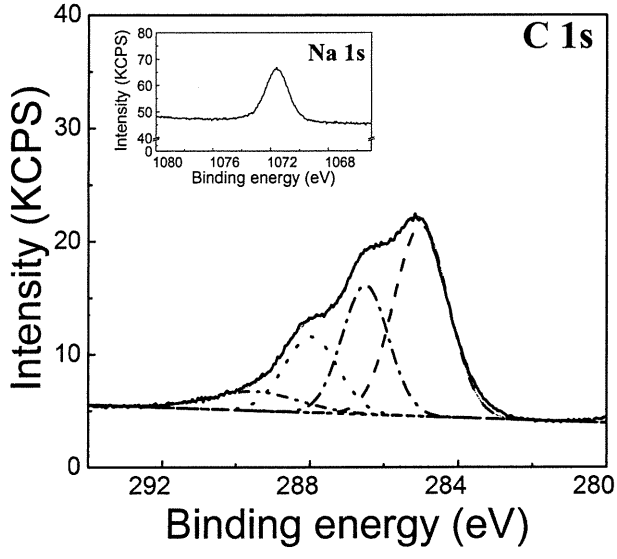

(d)

Figure 1. (Continued.)

However, no significant difference was observed in the XPS spectra of the two surfaces of HA/PIPAAm film cast on NTPSD.

3.2. Characterization of Gradient Structure of Films

The cross-section morphology and distribution of chemical composition along the thickness direction were investigated by means of SEM and EDX analysis, respectively. Figure 2 shows the EDX spectra of pure HA, pure PIPAAm, SEM

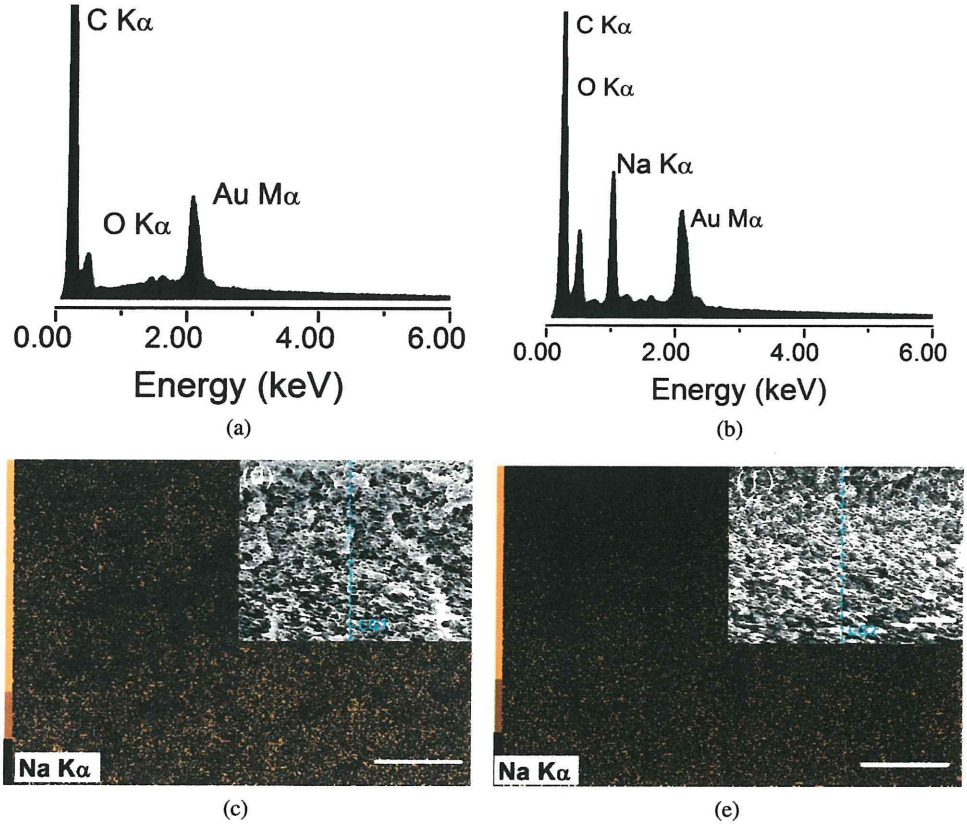

Figure 2. (a) EDX spectrum of pure PIPAAm film. (b) EDX spectrum of pure HA film. (c) EDX mapping measurements for Na on a freeze-fractured cross-section of the film cast on NTPSD. The inset (d) is the corresponding SEM image. (e) EDX mapping measurements for Na on a freeze-fractured cross-section of the film cast on PTPSD. The inset (f) is the corresponding SEM image. Scale bar = 100 μm. This figure is published in colour in the online edition of this journal, that can be accessed *via* http://www.brill.nl/jbs

micrographs of the cross-sections and EDX mapping measurements of Na for the two films cast on NTPSD and PTPSD. In Fig. 2 light areas correspond to a high concentration of Na atoms, and dark areas to a low concentration. It is clearly observed that the distribution of Na atoms, which is a probe element of HA, gradually changes along the thickness direction of the film cast on PTPSD, while no significant changes were observed for the film cast on NTPSD in ambient conditions. The results of EDX mapping for Na atoms strongly indicate that the composition of HA and PIPAAm gradually changes along the film thickness direction.

3.3. Surface Analyses of NTPSD, PTPSD and Formation of Gradient Structure

As shown in Fig. 3a and 3b, the characteristic surface property of PTPSD is much more hydrophilic due to the added functionally oxidized groups on the surface by oxygen plasma treatment. The mechanism of spontaneous formation of the compo-

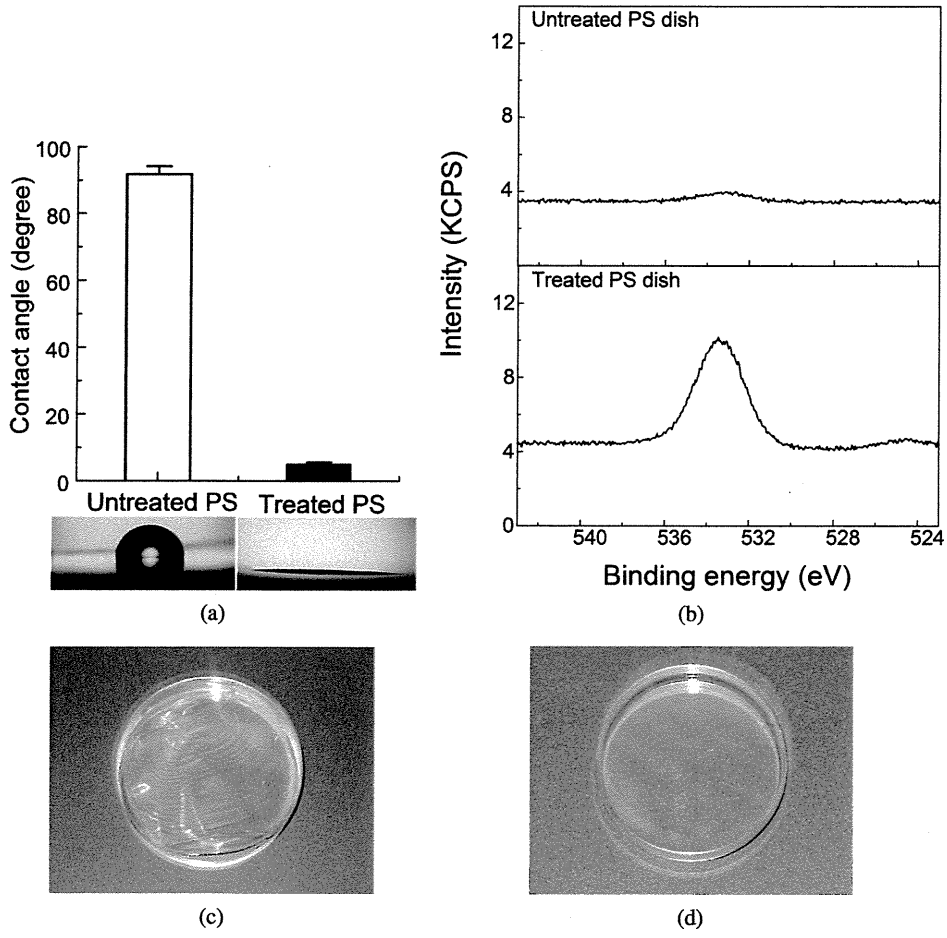

Figure 3. (a) Hydrophilicity measured by the contact angle of a water drop with NTPSD and PTPSD. Representative images are shown below. (b) XPS spectra in the O_{1s} core level region of the NTPSD and PTPSD surfaces. (c, d) The resulting film cast on NTPSD and PTPSD in vacuum conditions, respectively.

sitional gradient structure in PIPAAm/HA blend film on PTPSD was further studied by casting the film in vacuum condition. As shown in Fig. 3c and 3d, the film formed on NTPSD in vacuum is detached from the dish, while the film formed on PTPSD in vacuum is adhered on the dish. Both the high-resolution C_{1s} and Na_{1s} XPS spectra of the two surfaces of the film cast on NTPSD in vacuum conditions are also different from each other, but only show HA/PIPAAm blends with different compositional fractions (Fig. 4a and 4c). The air-side surface is a HA/PIPAAm blend rich in PIPAAm, and the dish-side surface is a HA/PIPAAm blend rich in HA. However, for the film cast on PTPSD in vacuum, the air-side surface shows completely the same XPS spectra as those of PIPAAm, and the dish-side surface shows XPS spectra extremely close to those of HA (Fig. 4b and 4d).

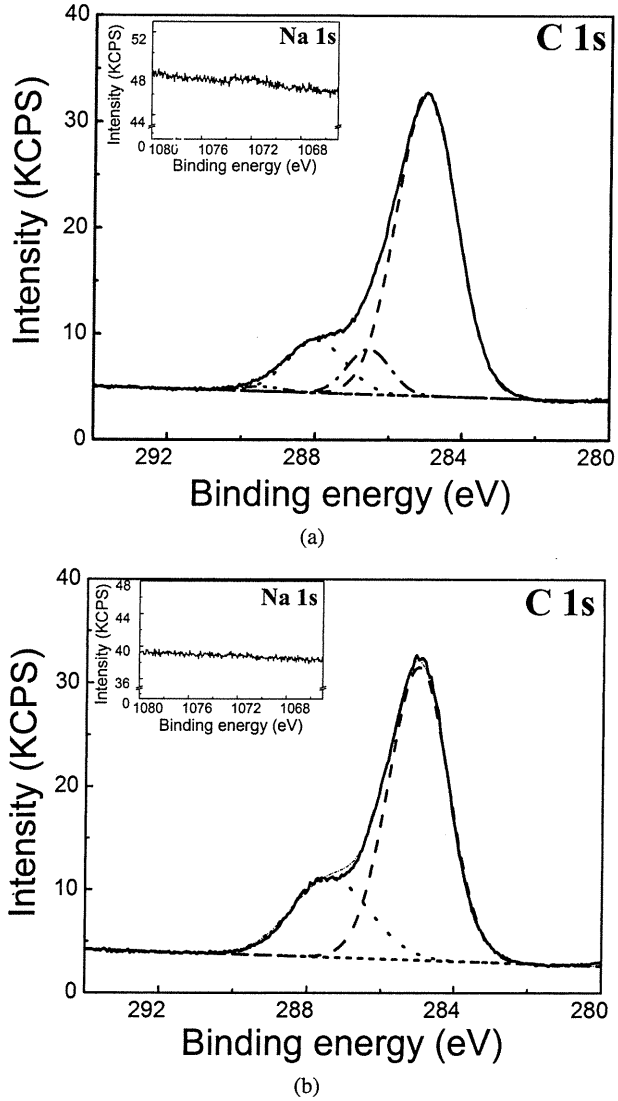

Figure 4. (a, c) XPS spectra of the C_{1s} core level region of the air-side and dish-side surfaces of the film cast on NTPSD in vacuum conditions, respectively. The insets are the corresponding Na_{1s} core level regions. (b, d) XPS spectra if the C_{1s} core level region of the air-side and dish-side surfaces of the film prepared on PTPSD in vacuum conditions, respectively. The insets are the corresponding Na_{1s} core level regions.

The characterization of the compositional distribution along the thickness direction of HA/PIPAAm films prepared under vacuum conditions on NTPSD and PTPSD was performed by means of step-scan PAS–FT-IR, SEM and EDX mapping measurement (Fig. 5). The step-scan PAS–FT-IR is a non-destructive, non-contact method with controllable sampling depth and needs little or no sample prepara-

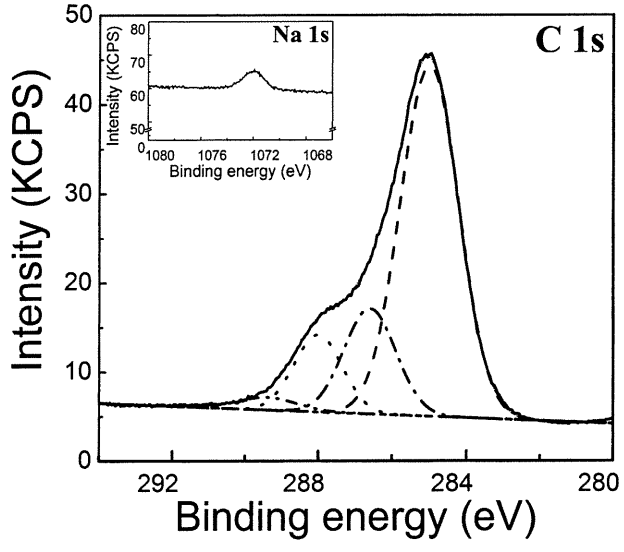

(c)

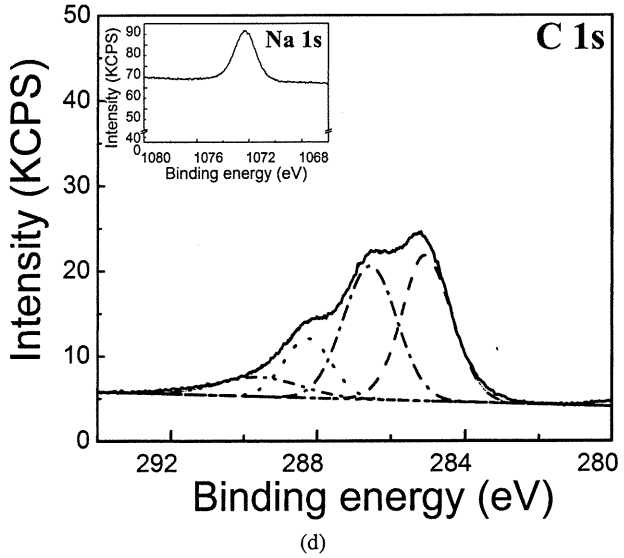

(d)

Figure 4. (Continued.)

tion. The results of PAS–FT-IR spectroscopy of increasing shallow-sampling depth corresponding to different mirror velocities of 1.0, 2.0 and 5.0 mm/s indicate that the fractions of HA and PIPAAm gradually change from the surfaces to the inside of the film for both films cast on NTPSD and PTPSD (Fig. 5a and 5b). The EDX mapping measurements for Na reveal that the HA fraction gradually decreases from the dish-side to the air-side of the film cast on PTPSD, while for the film cast on NTPSD, no such obvious change was observed on the cross-section. In order to

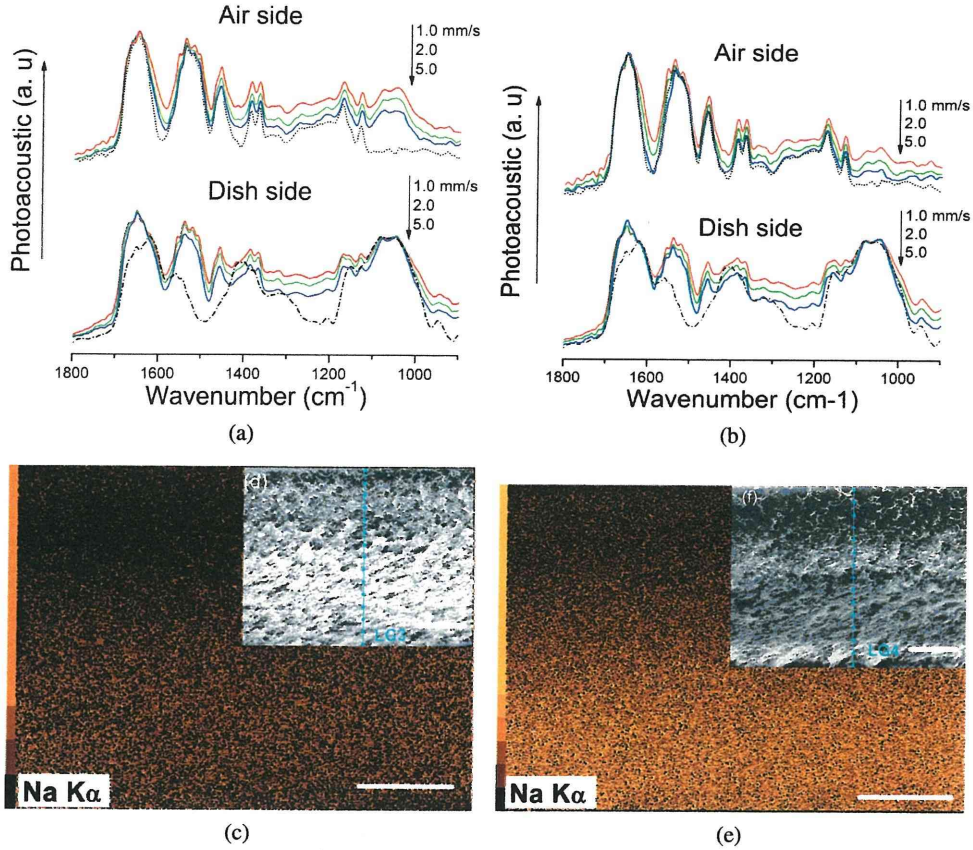

Figure 5. (a, b) PAS–FT-IR spectra with increasing shallow-sampling depth corresponding to mirror velocities of 1.0, 2.0 and 5.0 mm/s from the two surfaces of the films cast on NTPSD and PTPSD in vacuum conditions, respectively. The dotted and dash-dotted line correspond to the PAS–FT-IR spectra of pure PIPAAm and pure HA, respectively. (c, d) EDX mapping for Na and SEM image of the cross-section of the film cast on NTPSD in vacuum. (e, f) EDX mapping for Na and SEM image of the cross-section of the film cast on PTPSD in vacuum. Scale bar = 100 μm. This figure is published in colour in the online edition of this journal, that can be accessed *via* http://www.brill.nl/jbs

elucidate the contribution of the oxidized hydrophilic surface and acceleration of water molecules evaporation rate for the formation of compositional gradient structure in the HA/PIPAAm blend system, the degree of graduation of films has been plotted for mass content distribution of Na element along the thickness direction in different preparation conditions, ambient and vacuum conditions, on PTPSD and NTPSD, respectively. It is indicated that both the oxidized hydrophilic surface and evaporation rate of water molecules contribute to the formation of an ideal gradient structure in the HA/PIPAAm blend system (Fig. 6).

The formation mechanism of the compositional gradient structure in HA and PIPAAm blend system is a complicated process, related to the solubility parameters of two components, water-mediated and intermolecular hydrogen bonding network in

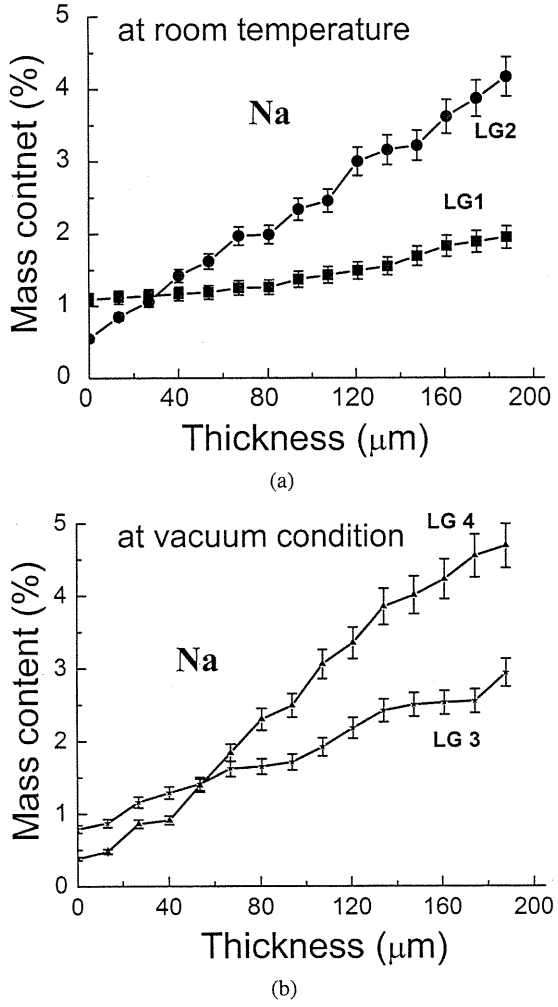

Figure 6. (a) EDX line scan results of Na on the cross-sections of films prepared in ambient conditions (LG1 for the film cast on NTPSD and LG2 for the film cast on PTPSD), (b) EDX line scan results of Na on the cross-sections of films prepared in vacuum conditions (LG3 for the film cast on NTPSD and LG4 for the film cast on PTPSD).

the blend system, and their rearrangement during the solvent evaporation process. In the homogeneous solution, the water-mediated or direct intermolecular hydrogen bonds between the functional groups of HA chain and oxidized functional groups on the PTPSD surface are constantly breaking and reforming at the urgings of thermal motion. However, because its intrinsic molecular structure, the PIPAAm chain hardly interacts with oxidized functional groups on the surface of PTPSD. In addition, the high solubility and mobility of PIPAAm makes it easy to accompany the evaporation of water molecules to move toward the air-side under the water molecule's plasticizing effect. In contrast, HA chains contain two kinds of links. The

glycosidic link between two rigid units consists of a single oxygen atom joining one sugar to the next, and each glucuronate unit carries a strong proton acceptor group associated with its carboxylate group. The unique molecular structure leads to the formation of a tape-like secondary structure and enables aggregation *via* specific interaction in water to form a meshwork, even at low concentrations [27, 28]. Therefore, once the intermolecular hydrogen bonding interaction was formed between carboxylate groups of HA and oxidized functional groups on the PTPSD surface, the water molecules' motion was not sufficient for breaking the interaction at high concentrations of HA during the evaporation process. Thus, HA molecules meshworks begin to overlap and aggregate on the PTPSD surface, resulting in changes of the film composition along the thickness direction and air-side and dish-side composition of the film, much the same as with pure PIPAAm and HA, respectively. However, on the hydrophobic surface of NTPSD, there is no strong interaction between the two components and the normal PS surface, such as intermolecular hydrogen bonds. Therefore, overlapping and aggregation of HA molecular meshworks occur in the whole mixture system under dominant contribution of entanglement, water-mediated and intermolecular interaction between HA and PIPAAm chains. The acceleration of the water molecular evaporation rate induces the delay of overlapping of HA molecular meshworks, resulting in the compositional difference between the two sides of the film. The fact that the resulting film on PTPSD, but not on NTPSD, is weakly adhered on the substrate indicates that the interactions between two components and oxidized surface of substrates are a significant factor for the formation of the gradient structure.

4. Conclusion

We prepared and characterized the compositional gradient structure in a HA/PIPAAm blend film. The formation mechanism of the functional gradient structure in a polysaccharide/polymer blend film self-organized from a homogeneous aqueous solution on PTPSD has been investigated by controlling the surface property of the casting substrate and the water evaporation rate. The gradient structure was confirmed by EDX mapping measurements for Na on the cross-section of the films and PAS–FT-IR analysis with increasing shallow-sampling depth from the two surfaces. The method of casting from a homogeneous aqueous solution is quite a simple way to prepare functional gradient polymeric materials. However, the mechanism involved in the formation of gradient structure is a complicated process related to the intrinsic properties of the components, the substrate properties and the solvent evaporation rate, indicating that with a suitable combination of these factors it can lead to polymeric composite materials with variable structures and properties.

References

1. H. A. Bruck, J. J. Evans and M. L. Peterson, *Exp. Mech.* **42**, 361 (2002).
2. L. L. Hench and J. M. Polak, *Science* **295**, 1014 (2002).